Journal Pre-proof

Salisbury screen with lossy nonconducting materials: way to increase spectral selectivity of absorption

V.V. Medvedev, N.N. Novikova, E. Zoethout

PII: S0040-6090(22)00147-X
DOI: https://doi.org/10.1016/j.tsf.2022.139232
Reference: TSF 139232

To appear in: *Thin Solid Films*

Received date: 17 August 2021
Revised date: 5 April 2022
Accepted date: 5 April 2022

Please cite this article as: V.V. Medvedev, N.N. Novikova, E. Zoethout, Salisbury screen with lossy nonconducting materials: way to increase spectral selectivity of absorption, *Thin Solid Films* (2022), doi: https://doi.org/10.1016/j.tsf.2022.139232

Highlights:

- A modified Salisbury screen design using lossy nonconducting layers is proposed.
- Total absorption conditions are derived for the modified Salisbury screen.
- Proof-of-principle Ge/Si/Al structures prepared.
- Narrow-band absorption in the near-infrared range demonstrated.

Salisbury screen with lossy nonconducting materials: way to increase spectral selectivity of absorption

V.V. Medvedev* and N.N. Novikova
Institute of Spectroscopy of the Russian Academy of Science, Fizicheskaya str. 5, Troitsk, Moscow 108840, Russia

E. Zoethout
DIFFER - Dutch Institute for Fundamental Energy Research, De Zaale 20, 5612 AJ Eindhoven, The Netherlands

(Dated: April 8, 2022)

We present a modified Salisbury screen design in which the thin absorbing metal layer is replaced with a layer of nonconducting lossy material. The conditions for total absorption in such a structure are explained using a simplified analytical model and rigorous numerical calculations. For the proof-of-principle experiments, germanium/silicon bilayers deposited on aluminium substrates are designed and manufactured. The structures demonstrate nearly perfect absorption in the near-IR spectral range. Compared to conventional Salisbury screens, a lossy semiconductor top layer exhibits increased spectral selectivity of absorption. The wavelength of nearly perfect absorption remains tunable by optimizing the thicknesses of the lossy and transparent layers.

I. INTRODUCTION

Studies of structures based on optical interference coatings exhibiting high radiation absorption have attracted much attention in the recent decade [1–25]. Such structures are in demand for many applications, including photovoltaic cells, radiation detectors, sensors, thermal emitters, and color filters [26–33]. One of the fundamentally important absorber structures based on interference coatings is a so-called Salisbury screen [34]. Figure 1 schematically shows a Salisbury screen consisting of a lossless spacer layer (2) placed between a metal back reflector (3) and a lossy thin metal layer (1). The Salisbury screen exhibits high absorption due to destructive interference of incident and reflected waves. The approximate analytical conditions for total absorption of monochromatic radiation with a wavelength λ by the Salisbury screen are expressed as:

$$n_1 = \kappa_1, \tag{1a}$$

$$d_1 = \lambda/(4\pi n_1 \kappa_1), \tag{1b}$$

$$d_2 = \lambda/4n_2, \tag{1c}$$

where n_1, κ_1, and d_1 are the refractive index, extinction coefficient, and thickness of the upper metal layer, respectively; and n_2 and d_2 are the refractive index and thickness of the spacer layer. According to Eqs. 1, the optimal optical thickness of the transparent layer is a quarter wavelength, and the optimal thickness of the upper metal layer at characteristic values of n_1 and κ_1 is in the nanometer scale.

Equations 1 define the conditions for total absorption at a certain wavelength. A change in the wavelength at fixed parameters of the Salisbury screen structure leads to the violation of the destructive interference condition, and, as a consequence, to nonzero incident wave reflection. Thus, the interference-enhanced absorption peak of the Salisbury screen has a certain finite bandwidth. The absorption bandwidth can be increased by adding additional dielectric-metallic bilayers, resulting in multilayered structures known as Jaumann absorbers [35]. The absorption peak width of the Salisbury screen can be reduced by using polar dielectric substrates [22], by introducing additional transparent dielectric layers into the structure [36], or by using additional spectral filters [37, 38]. It should be noted that there are also other types of light-absorbing interference coatings with high spectral absorption selectivity. For example, Yen and Chung[14] proposed a design of a narrow-band terahertz radiation absorber based on a single layer of a polar dielectric coating deposited on a metal substrate. A polar dielectric allows one to use phonon-assisted absorption. At the same time, optimization of the coating thickness makes it possible to obtain a narrow absorption band at a certain wavelength within the Restrahlen band of the selected coating material. This type of coating, in contrast to the Salisbury screen, does not allow the resonant absorption wavelength to be selected in an arbitrary way: the wavelength can only be changed by changing the coating material. It should also be noted that phonon-assisted absorption in polar materials occurs in the mid- and far-IR ranges, which is impossible in the visible and near-IR ranges. For the latter spectral ranges, narrow-band absorbers based on metal-dielectric metasurfaces are developed [39–42], and the search for new designs of light-absorbing coatings for the visible and near-IR ranges with high spectral selectivity remains relevant.

In this paper, we revise the light absorbing properties of the Salisbury screen. Using an analytical model, we analyze the conditions for absorption of monochromatic radiation and show that not only metals, but also dielectrics and semiconductors with nonzero losses can

* v.medvedev@rnd-isan.ru

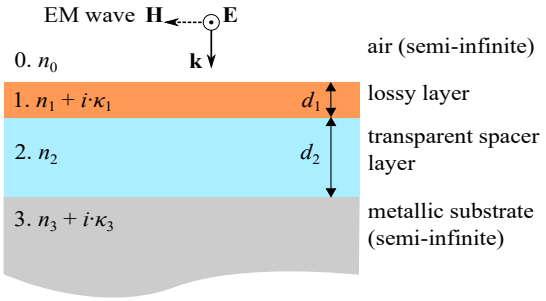

FIG. 1. Schematic of a two-layer coating (lossy layer and lossless layer) on an optically thick metal substrate.

be used as an absorber material in the Salisbury screen. We provide examples of such materials. In particular, we show that germanium is a suitable material for fabricating absorbers for near-IR radiation. Using accurate calculations, we compare the properties of Salisbury screens with metallic and nonmetallic absorbers. Our calculations show that a nonmetallic absorber makes it possible to reduce the spectral width of the absorption peak in comparison with a metallic absorber. Finally, test structures are fabricated using a common physical vapor deposition technique to experimentally demonstrate nearly perfect narrow-band absorption of near-IR radiation. Such structures are believed to replace more difficult-to-manufacture absorbers based on metal-dielectric metasurfaces.

II. TOTAL ABSORPTION CONDITIONS: SIMPLIFIED ANALYTICAL THEORY

First, we formulate the conditions for total absorption of a monochromatic plane wave by the structure in question. Because this structure has an opaque metal substrate, the absorption coefficient is defined as $A = 1-|r|^2$, where r is the amplitude reflection coefficient. The amplitude reflection coefficient of a two-layer interference coating is expressed as

$$r = \frac{r_{01} + r_{123}\exp(2ik_1d_1)}{1 + r_{01}r_{123}\exp(2ik_1d_1)}, \tag{2}$$

with

$$r_{123} = \frac{r_{12} + r_{23}\exp(2ik_2d_2)}{1 + r_{12}r_{23}\exp(2ik_2d_2)}, \tag{3}$$

where $r_{jl} = (\widetilde{n}_j - \widetilde{n}_l)/(\widetilde{n}_j + \widetilde{n}_l)$ is the Fresnel reflection coefficient, $k_j = 2\pi\widetilde{n}_j/\lambda$ is the wavenumber, λ is the wavelength of the incident radiation, d_j is the jth layer thickness, and $\widetilde{n}_j = n_j + i\kappa_j$ is the complex refractive index of the jth medium. Note that $\kappa_2 = 0$, i.e., $\widetilde{n}_2 = n_2$, since the second layer is considered transparent in our theoretical analysis.

The condition for total absorption at a wavelength λ can be obtained from the roots of the numerator of Eq. 2. For ease of analysis, the metal substrate is approximated by a perfect electrical conductor (PEC). Therefore, we can set $r_{23} = -1$. We consider the particular case of $d_2 = 0.25\lambda/n_2$ (i.e. $k_2d_2 = \pi/2$), which is used as the baseline in the Salisbury screen theory. In this case, $r_{123} = 1$ and the condition for zero reflection is simplified:

$$r_{01} + \exp(2ik_1d_1) = 0. \tag{4}$$

Equation 4 is equivalent to the two equations:

$$|r_{01}| = \exp(-4\pi\kappa_1d_1/\lambda), \tag{5a}$$
$$\arg(r_{01}) - 4\pi n_1d_1/\lambda = \pi(2m+1), \tag{5b}$$

where $m = 0, \pm1, \pm2, ...$ Equations 5 implicitly relate the optimal values of n_1, κ_1, and d_1. These equations can be solved using numerical methods. However, it is also useful to obtain an approximate analytical solution. Equation 5(b) can be rewritten in the form:

$$d_1 = \frac{\lambda}{4\pi n_1}(\arg(r_{01}) - \pi(2m+1)). \tag{6}$$

For lossy materials, the value of $\arg(r_{01})$ slightly exceeds π for most wavelengths. Hence, Eq. 6 provides positive values for d_1 only at $m \le 0$. The case of $m = 0$ corresponds to a conventional previously studied Salisbury screen (see Eqs. 1). We focus on the case of $m = -1$. Equation 6 with $\arg(r_{01}) \approx \pi$ yields $d_1 \approx \lambda/2n_1$. Hence, the optimal thickness of the top layer is close to half the wavelength in the medium. Absorption in such relatively thick layers can be achieved only using materials with relatively low values of the extinction coefficient, e.g., $\kappa_1 \sim 0.1$ [25]. Assuming $n_1 > 1$, the Fresnel reflection coefficient r_{01} can be approximated in this case as $r_{01} \approx (1-n_1)/(1+n_1)$. Equation 5(a) can now transform to the equation:

$$\kappa_1 = -\frac{\lambda}{4\pi d_1}\ln(|r_{01}|) \approx -\frac{n_1}{2\pi}\ln\left(\frac{n_1-1}{n_1+1}\right). \tag{7}$$

Note that Eq. 7 becomes invalid around $n_1 = 1$. At $n_1 \gg 1$, Eq. 7 is simplified to $\kappa_1 \approx 1/\pi$. Thus, we obtain the approximate equations for the total absorption conditions:

$$d_1 = \lambda/2n_1, \tag{8a}$$
$$d_2 = \lambda/4n_2, \tag{8b}$$
$$\kappa_1 = 1/\pi. \tag{8c}$$

In addition to the approximate analytical solution expressed by Eqs. (8), it is also possible to obtain the exact solution to Eqs. (5) for a given m. To do this, we used the methods of numerical solution of equations, implemented in the SciPy library for the Python programming language [43]. Figure 2 shows such a solution for $m = -1$ in the form of all possible combinations of n_1, κ_1 and $\delta_1 = n_1d_1/\lambda$, satisfying Eqs. (5). Note that, for simplicity of presenting the results, we will use

the wavelength-normalized optical thickness of the upper layer of the coating (δ_1), rather than the physical thickness (d_1). Figure 2(a) shows κ_1 as a function of n_1, calculated numerically (solid orange curve) by Eqs. 5 at $m = -1$ and obtained analytically (grey dashed lines) using Eqs. 8. Similarly, Fig. 2(b) displays the reduced optical thickness ($n_1 d_1/\lambda$) as a function of n_1, calculated numerically (solid orange curve) by Eqs. 5 at $m = -1$ and obtained analytically (grey dashed lines) using Eqs. 8. It is seen that the approximate analytical solution works reasonably well for $n_1 > 2$, i.e. in the range of refractive indices typical for most lossy dielectrics and semiconductors. In this case, the optimal extinction coefficient of the top layer is $\kappa_1 \approx 0.32$ and the optimal thickness slightly exceeds half the wavelength. It is also worth noting that according to Fig. 2a, total absorption can also be achieved using materials with $n_1 < 1$ and $\kappa_1 < 1$, i.e. index-near-zero materials. However, in this case, the reduced optical thickness δ_1 increases to almost 0.75.

It should also be noted that in a similar way one can obtain approximate analytical and numerical solutions to Eqs. (5) for $m < -1$. In this case, the optimal values of κ_1 decrease with decreasing m, while the optimal values of δ_1, on the contrary, increase.

The numerical analysis shows that zero reflection can also be achieved with other values of d_2 (i.e. $d_2 \neq 0.25\lambda/n_2$) as well as with other values of r_{23}, corresponding to metal substrates. This however results in only relatively small changes in the optimal parameters (n_1, κ_1 and d_1) of the upper layer.

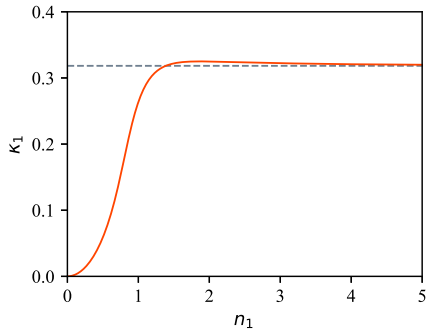

(a)

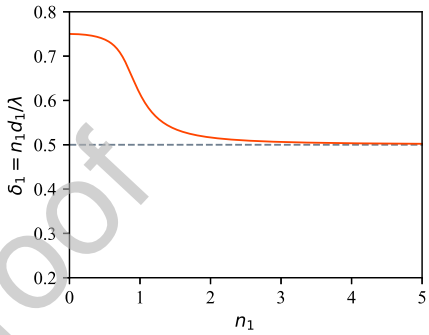

(b)

FIG. 2. Dependences of (a) the extinction coefficient and (b) reduced optical thickness on the refractive index for the considered two-layer coating on a PEC substrate at a wavelength λ. The thickness of the transparent layer is set at $d_2 = 0.25\lambda/n_2$. The solid orange curves represent the results of the numerical solution to Eqs. 5 at $m = -1$; dashed grey lines show the approximate analytical solution by Eqs. 8.

III. TOTAL ABSORPTION CONDITIONS: REAL MATERIALS AND RIGOROUS CALCULATIONS

At this point we consider properties of real materials for designing the described bilayer structures. The calculated optimal values of the complex refractive index (Fig. 2(a)) of the top layer are similar to those of semiconductors in the vicinity of their bandgap or to polar dielectrics around their Restrahlen bands. For example, suitable values for the complex refractive index can be found for silicon (Si) and germanium (Ge) in the visible and near-IR ranges at around their bandgaps [44, 45]. In the mid- and far-IR ranges, suitable optical constants can be found in compounds such as silicon carbide (SiC), silicon nitride (SiN_x), aluminum nitride (AlN), and gallium arsenide (GaAs) at around their Restrahlen bands [46–48].

Let us consider an example of the design of an absorber for near-IR radiation based on a two-layer Ge-on-Si coating deposited on an aluminum (Al) substrate. In rigorous calculations of the reflectance and absorptance of layered structures, we use the transfer matrix method [49]. In the calculations, we use optical constants of materials obtained on the basis of ellipsometric measurements (see Section IV) and literature data [50]. For given materials constituting the considered structure, its reflectance $R = |r|^2$ at a wavelength λ is governed only by the layer thicknesses, d_1 and d_2. Figure 3(a) shows an example of the calculated reflection coefficient of a Ge coating at a wavelength of 1170 nm. Using numerical optimization, one can find the optimal values of d_1 and d_2 at which the reflection becomes minimal. To this end, we use the numerical optimization routines implemented in the SciPy library for the Python programming language [43]. At $\lambda = 1170$ nm, the calculations for the considered Ge/Si/Al structures yield $R = 0$ at $d_1 \approx 114$ nm ($d_1 \approx 0.47\lambda/n_1$) and $d_2 \approx 76$ nm ($d_2 \approx 0.25\lambda/n_2$). The corresponding point (d_1,d_2) is shown by a white cross in Fig. 3(a). Note that at the selected wavelength, the obtained optical thicknesses of the layers are close to those predicted by Eqs. 8. Next, by varying the wavelength and repeating the described procedure for minimizing R, one can find the spectral range in which total absorption of monochromatic radiation can be achieved. Figure 3(b) shows the calculated dependence of $R_{\min}$ on λ. One can see that total absorption can be achieved at any wavelength from the 9441266 nm range. Figures 3(c)-

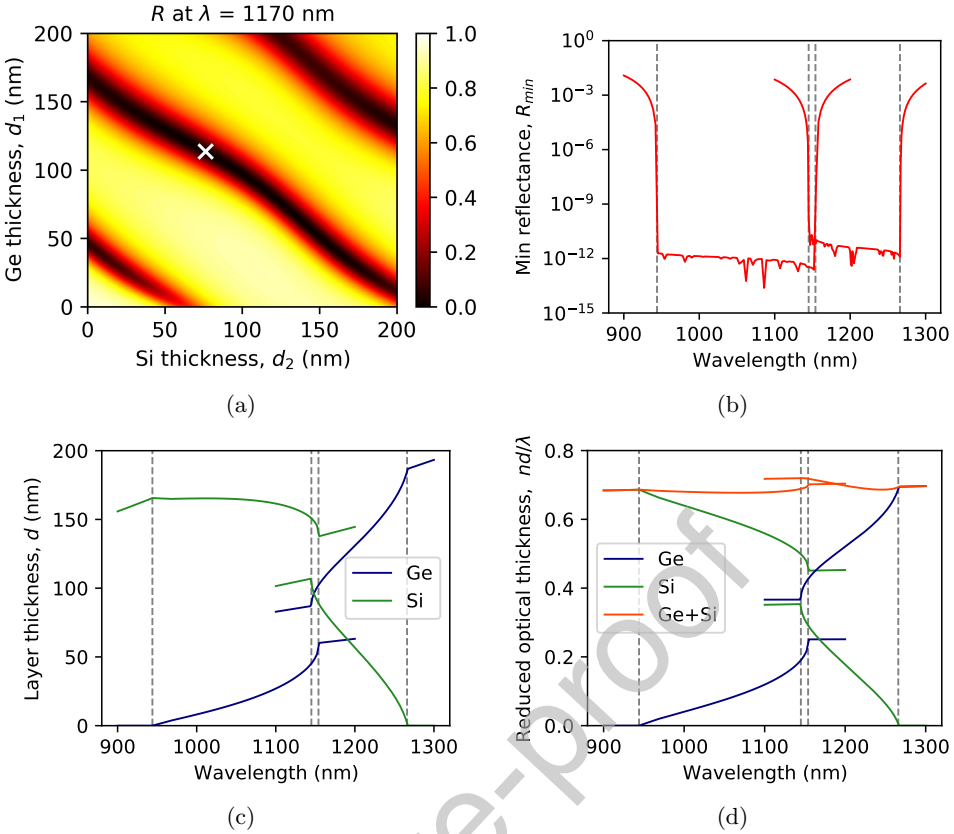

FIG. 3. (a) Calculated reflectivity of 1170 nm radiation normally incident on a Ge/Si/Al structure as a function of the Ge and Si layer thicknesses, d_1 and d_2. The white cross indicates the point ($d_1 \approx 114$ nm and $d_2 \approx 76$ nm) of $R = 0$. (b) Dependence of the minimum reflectance ($R_{\min}$) of Ge/Si/Al structures on the wavelength in the near-IR range. Vertical dashed lines at $\lambda = 944$ nm and $\lambda = 1266$ nm show the spectral range where zero reflectance can be achieved. Vertical dashed lines at $\lambda = 1145$ nm and $\lambda = 1154$ nm display the spectral range where zero reflectance can be achieved for different combinations of the layer thicknesses. (c) Optimum Ge and Si layer thicknesses corresponding to the minimum reflectance of the Ge/Si/Al structure as a function of wavelength. The Ge thickness is represented by solid blue curves, and the Si thickness is represented by solid green curves. (d) Optimal optical thicknesses of Ge and Si layers and their sum normalized to the wavelength. The Ge thickness is represented by solid blue curves, the Si thickness is represented by solid green curves, and the total thickness is represented by solid orange curves.

(d) show the wavelength dependence of the optimal layer thicknesses and the optimal reduced optical layer thicknesses (nd/λ). It can be seen that at the boundaries of the range, one of the structure layers vanishes, i.e. the coating becomes single layered. One can also see that the total optical thickness of the coating does not exceed 0.72λ in the entire range. Interestingly, in the spectral range from 1145 to 1154 nm, total absorption is achieved at two different combinations of layer thicknesses, d_1 and d_2.

Now we will analyze the absorption spectra of the considered Ge/Si/Al structures. Figure 4(a) shows the calculated absorption spectra for a structure with layer thicknesses optimized for total absorption at $\lambda = 1170$ nm. In Fig. 4(a), the blue dashed curve shows the absorption spectrum in the Ge layer, the orange dash-dotted curve presents the absorption spectrum in the Si layer, the green dotted line illustrates the absorption spectrum in the Al substrate, and the solid red curve demonstrates the integral absorption spectrum. Calculations show that at the target wavelength of 1170 nm, about 75% of the radiation is absorbed in the Ge layer, with the remaining 25% of the absorbed radiation being divided approximately equally between the Si layer and the Al substrate. It is also important to compare the spectral characteristics of the considered Ge/Si/Al structures with the characteristics of the Salisbury screen based on a metal absorbing layer. We choose chromium (Cr) as an absorbing metal, which is often used for such purposes. The optical constants of chromium can be found elsewhere [50]. We use again the wavelength of 1170 nm. According to our calculations, total absorption in Cr/Si/Al at this wavelength is achieved at Cr and Si layer thicknesses of $d_1 \approx 6$ nm and $d_2 \approx 62$ nm, respectively. Figure 4(b) compares the absorption spectra of Ge/Si/Al and Cr/Si/Al structures optimized for

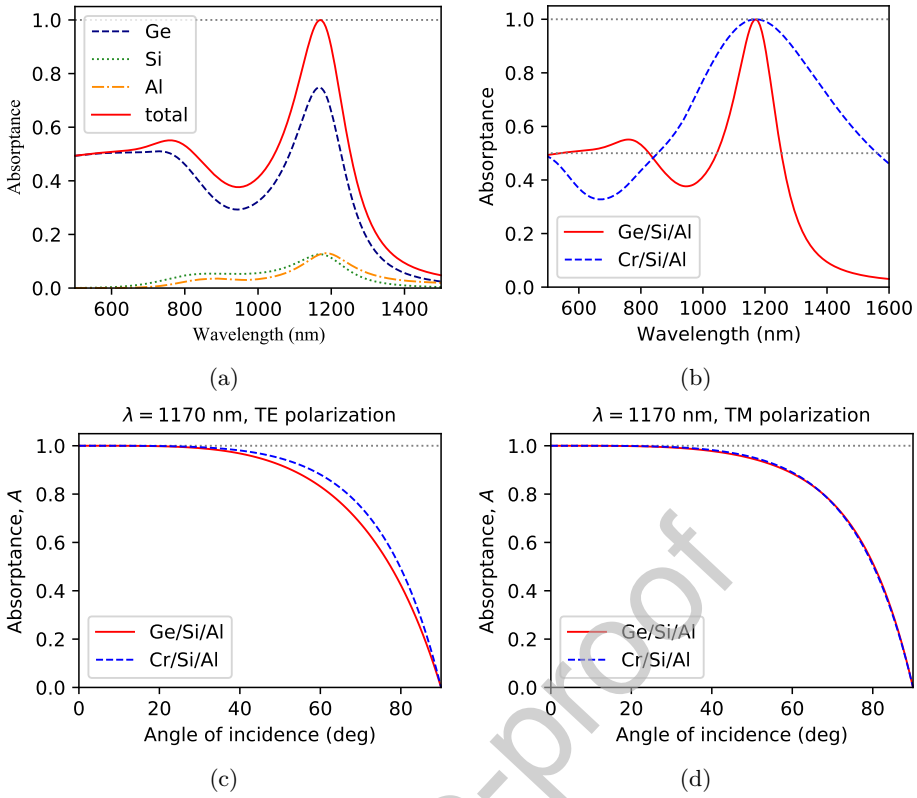

FIG. 4. (a) Calculated absorption spectra for the Ge/Si/Al structure with layer thicknesses optimized for total absorption at a wavelength of 1170 nm. The blue dashed curve is the absorption in the Ge layer, the green dotted curve is the absorption in the Si layer, the orange dot-dashed curve is the absorption in the Al substrate, and the solid red curve is the total absorption in the structure. (b) Calculated absorption spectra of Ge/Si/Al (solid red curve) and Cr/Si/Al (dashed blue curve) structures with layer thicknesses optimized for total absorption at 1170 nm. (c) - (d) Comparison of angular dependences of radiation absorption by Ge/Si/Al (solid red curve) and Cr/Si/Al (dashed blue curve) structures at a wavelength of 1170 nm in the case of TE and TM polarizations.

total absorption at the selected wavelength. According to the calculations, the full width of the absorption peak at its half maximum for the Cr/Si/Al structure is approximately 709 nm, and for the Ge/Si/Al structure it is approximately 208 nm, which is almost 3.5 times narrower. Let us now compare the angular dependences of the absorptance for Ge/Si/Al and Cr/Si/Al structures at a fixed wavelength. Figures 4(c)-(d) show the corresponding calculation results for structures with layer thicknesses optimized for total absorption of radiation normally incident at $\lambda = 1170$ nm. It can be seen from Figs. 4(c)-(d) that the angular dependences of the absorptance for both structures are very close: in the case of TM polarization (Fig. 4(d)), they almost coincide, and in the case of TE polarization (Fig. 4(c)), the maximum difference in absorption is $A_{\mathrm{Cr/Si/Al}} - A_{\mathrm{Ge/Si/Al}} \approx 0.075$, observed according to the calculations at an angle of incidence of about 75°.

IV. EXPERIMENTAL DEMONSTRATION

To experimentally demonstrate the absorption of light by such a modified Salisbury screen, we have fabricated several samples of Ge/Si/Al coated structures and additional single layer Ge and Si coated structures. In order to assure the same chemical state of the material under investigation, all samples were prepared in an ultra-high vacuum (UHV) environment with a base pressure better than $1 \cdot 10^{-6}$ Pa. Layers were deposited at room temperature onto the substrates by physical vapour deposition (electron beam evaporation). A quartz crystal microbalance (QCM) was used to control the amount of the deposited material (±1% of the reported values). The QCM measures a change in the mass transferred into nominal layer thickness. This nominal layer thickness incorporates an amount of the material that adds up to this thickness at a bulk density (Ge: 5.35 g/cm^3, Si: 2.3 g/cm^3).

First, single layer samples were characterized *ex-situ* with grazing incidence X-ray reflectometry (XRR). Grazing incidence X-ray reflection (Cu K-α) was measured

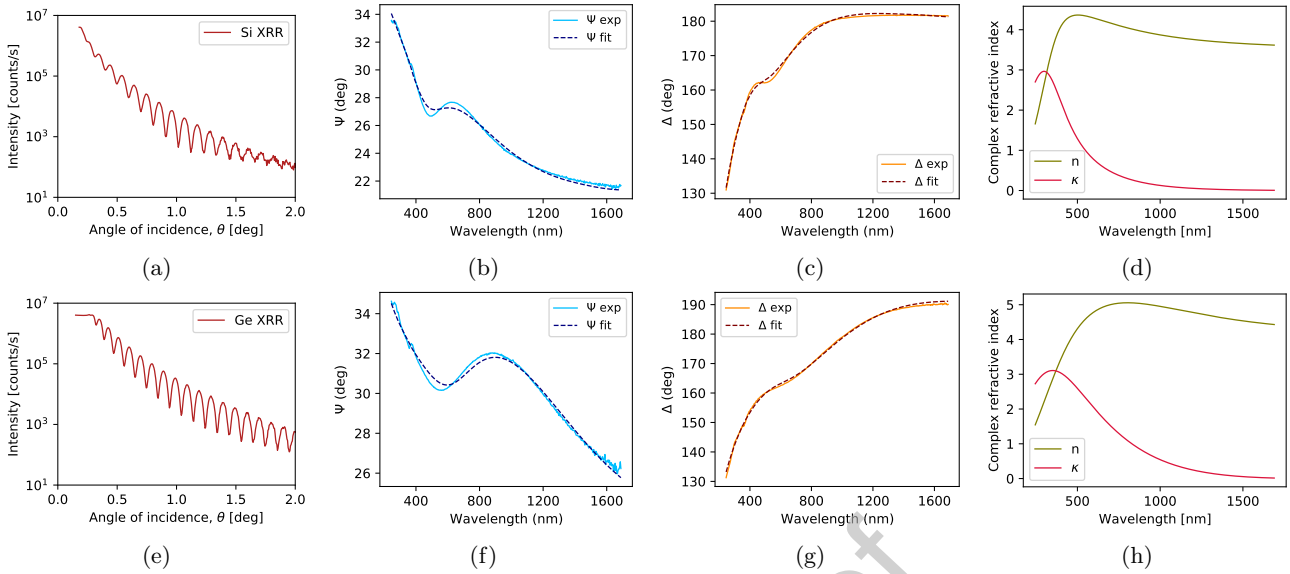

FIG. 5. (a) Grazing incidence XRR for 40 nm Si single layer coating samples; (b)-(c) ellipsometer data for Ψ and Δ parameters and the model fit for a 40-nm-thick Si sample; (d) complex refractive index of the 40-nm-thick Si sample retrieved from the model fit; (e) grazing incidence XRR for 42 nm Ge single layer coating samples; (f)-(g) ellipsometer data for Ψ and Δ parameters and the model fit for a 42-nm-thick Ge sample; (h) complex refractive index of the 42-nm-thick Ge sample retrieved from the model fit.

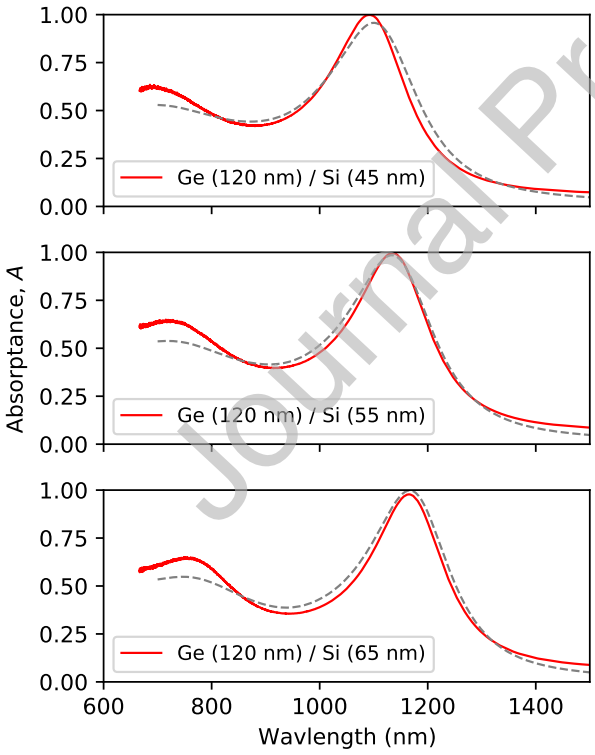

FIG. 6. Measured (solid red curved) and calculated (grey curved) absorption spectra for Ge/Si/Al structures with a fixed Ge layer thickness of 120 nm and Si layer thicknesses of 45 nm (top), 55 nm (middle) and 65 nm (bottom).

with a Bruker D8 eco. XRR measurements of thin films can be used to determine film properties like layer thickness and interface roughness, but here they were used to determine the tooling factor of the QCM of the coating setup. Figures 5(a,e) show an example of XRR measurements at 1° fixed source angle for a single layer Ge and Si coating on a silicon wafer. The films show a number of oscillations in the theta range of $0.5° - 2°$. The periodicity of the oscillations can be interpreted via Braggs law to a layer thickness. The measurement results presented in Figs. 5(a,e) present XRR measurements for the Ge and Si layers, which have thicknesses of 42 nm and 40 nm, respectively. Films made of materials with small amounts of atmospheric oxidation (silicon and germanium in our case) and having a thickness in the range of 20 to 50 nm are ideal to determine the QCM tooling factor.

Second, optical properties of the Si and Ge single layer coating samples were characterized by a Woollam M2000 FI spectroscopic ellipsometer with a spectral range of 250-1700 nm. The ellipsometer was used at 60° angle of incidence with respect to the surface normal. A layered system consisting of the silicon wafer substrate and the respective single layer, both including a thin native oxide, have been modelled to fit the experimental data. In the case of the single layers, use was made of the Tauc-Lorentz and Cody-Lorentz shape to approximate Ge and Si layers, respectively. The single layer model thickness was constrained to approximate the XRR calibrated deposition value within a few percent. Figures 5(b,c) and 5(f,g) show the measured and modeled ellipsometer parameters for 40-nm-thick Si and 42-nm-thick Ge layers, respectively. The model fits well the data. Figures 5(d,h)

illustrate the optical properties of the samples. The chosen shape indicates that the model fits the data smoothly. All optical properties extracted from ellipsometer data resulted from a fit with a mean square error (MSE) of 0.7-1% between data and model. The modeled silicon and germanium layer properties are close to those cited in the literature, but not identical. This could be caused by the fact that modeled optical properties of thin layers have a larger error than opaque layers, but it might also reflect the differences in the optical response between them.

Finally, for an experimental demonstration of the operation of the Ge/Si/Al Salisbury screen, three coating samples were manufactured with a fixed thickness (120 nm) of the Ge layer and three different thicknesses (45 nm, 55 nm and 65 nm) of the Si layer. Reflection spectra of the samples were measured using a Bruker IFS 66 v/s FTIR spectrometer. A protected silver mirror (THORLABS PF10-03-P01) was used as a reference sample in the measurements. According to the specification, this mirror guarantees an average reflectance above 97% in the 0.452.0 μm wavelength range. The measurements were carried out using an unpolarized radiation beam incident on the surface of a sample at an angle of 13° with respect to the surface normal. The measured spectra are shown with red solid curves in Fig. 6. The grey dashed curves in Fig. 6 represent the calculated spectra for the given layer thicknesses of the fabricated samples. One can see that the results of calculations and measurements are in reasonable agreement. According to the measurement results, the strongest absorption ($A \approx 0.998$) is achieved for the Ge(120 nm)/Si(55 nm)/Al structure at a wavelength $\lambda \approx 1094$ nm. Thus, we have experimentally demonstrated near-unity absorption at an arbitrary wavelength from the spectral range (9441266 nm, see section III), in which the Salisbury screen based on Ge/Si/Al coatings works effectively.

V. CONCLUSIONS

We have described the condition for total absorption of radiation by a Salisbury-screen-type structure in which a thin metal absorber film is replaced by a lossy semiconductor film. The use of this material allows the width of the resonance absorption peak to be substantially narrowed. We have also experimentally demonstrated almost total absorption of near-IR radiation by Ge/Si/Al coating samples. The proposed structure is promising for sensing and imaging applications.

[1] M. A. Kats, R. Blanchard, P. Genevet, F. Capasso, Nanometre optical coatings based on strong interference effects in highly absorbing media, Nature Materials 12 (1) (2013) 20. arXiv:https://doi.org/10.1038/nmat3443, doi:10.1038/nmat3443.
URL https://doi.org/10.1038/nmat3443

[2] M. A. Kats, D. Sharma, J. Lin, P. Genevet, R. Blanchard, Z. Yang, M. M. Qazilbash, D. N. Basov, S. Ramanathan, F. Capasso, Ultra-thin perfect absorber employing a tunable phase change material, Applied Physics Letters 101 (22) (2012) 221101. arXiv:https://doi.org/10.1063/1.4767646, doi:10.1063/1.4767646.
URL https://doi.org/10.1063/1.4767646

[3] M. A. Kats, F. Capasso, Optical absorbers based on strong interference in ultra-thin films, Laser & Photonics Reviews 10 (5) (2016) 735–749. arXiv:https://doi.org/10.1002/lpor.201600098, doi:https://doi.org/10.1002/lpor.201600098.
URL https://onlinelibrary.wiley.com/doi/abs/10.1002/lpor.201600098

[4] J. Park, S. J. Kim, M. L. Brongersma, Condition for unity absorption in an ultrathin and highly lossy film in a gires–tournois interferometer configuration, Optics Letters 40 (9) (2015) 1960–1963. arXiv:https://doi.org/10.1364/OL.40.001960, doi:10.1364/OL.40.001960.
URL https://doi.org/10.1364/OL.40.001960

[5] J. Park, J.-H. Kang, A. P. Vasudev, D. T. Schoen, H. Kim, E. Hasman, M. L. Brongersma, Omnidirectional near-unity absorption in an ultrathin planar semiconductor layer on a metal substrate, ACS Photonics 1 (9) (2014) 812–821. arXiv:https://doi.org/10.1021/ph500093d, doi:10.1021/ph500093d.
URL https://doi.org/10.1021/ph500093d

[6] D. Liu, H. Yu, Z. Yang, Y. Duan, Ultrathin planar broadband absorber through effective medium design, Nano Research 9 (8) (2016) 2354–2363. arXiv:https://doi.org/10.1007/s12274-016-1122-x, doi:10.1007/s12274-016-1122-x.
URL https://doi.org/10.1007/s12274-016-1122-x

[7] J. Rensberg, Y. Zhou, S. Richter, C. Wan, S. Zhang, P. Schöppe, R. Schmidt-Grund, S. Ramanathan, F. Capasso, M. A. Kats, et al., Epsilon-near-zero substrate engineering for ultrathin-film perfect absorbers, Physical Review Applied 8 (1) (2017) 014009. arXiv:https://doi.org/10.1103/PhysRevApplied.8.014009, doi:10.1103/PhysRevApplied.8.014009.
URL https://doi.org/10.1103/PhysRevApplied.8.014009

[8] W. Streyer, S. Law, G. Rooney, T. Jacobs, D. Wasserman, Strong absorption and selective emission from engineered metals with dielectric coatings, Optics Express 21 (7) (2013) 9113–9122. arXiv:https://doi.org/10.1364/OE.21.009113, doi:10.1364/OE.21.009113.
URL https://doi.org/10.1364/OE.21.009113

[9] L. J. Krayer, J. Kim, J. N. Munday, Near-perfect absorption throughout the visible using ultra-thin metal films on index-near-zero substrates, Optical Materials Express 9 (1) (2019) 330–338. arXiv:https://doi.org/10.1364/OME.9.000330, doi:10.1364/OME.9.000330.
URL https://doi.org/10.1364/OME.9.000330

[10] V. Medvedev, V. Gubarev, C. Lee, Optical performance of a dielectric-metal-dielectric antireflective absorber structure, JOSA A 35 (8) (2018) 1450–1456. arXiv:https://doi.org/10.1364/JOSAA.35.001450, doi:10.

1364/JOSAA.35.001450.
URL https://doi.org/10.1364/JOSAA.35.001450

[11] S. S. Mirshafieyan, J. Guo, Silicon colors: spectral selective perfect light absorption in single layer silicon films on aluminum surface and its thermal tunability, Optics Express 22 (25) (2014) 31545–31554. arXiv:https://doi.org/10.1364/OE.22.031545, doi:10.1364/OE.22.031545.
URL https://doi.org/10.1364/OE.22.031545

[12] M. A. Badsha, Y. C. Jun, C. K. Hwangbo, Admittance matching analysis of perfect absorption in unpatterned thin films, Optics Communications 332 (2014) 206–213. arXiv:https://doi.org/10.1016/j.optcom.2014.07.004, doi:10.1016/j.optcom.2014.07.004.
URL https://doi.org/10.1016/j.optcom.2014.07.004

[13] M. R. S. Dias, C. Gong, Z. A. Benson, M. S. Leite, Lithography-free, omnidirectional, cmos-compatible alcu alloys for thin-film superabsorbers, Advanced Optical Materials 6 (2) (2018) 1700830. arXiv:https://doi.org/10.1002/adom.201700830, doi:10.1002/adom.201700830.
URL https://doi.org/10.1002/adom.201700830

[14] S.-T. Yen, P.-K. Chung, Far-infrared quasi-monochromatic perfect absorption in a thin GaAs film on gold, Optics Letters 40 (16) (2015) 3877–3880. arXiv:https://doi.org/10.1364/OL.40.003877, doi:10.1364/OL.40.003877.
URL https://doi.org/10.1364/OL.40.003877

[15] C. Valagiannopoulos, A. Tukiainen, T. Aho, T. Niemi, M. Guina, S. Tretyakov, C. Simovski, Perfect magnetic mirror and simple perfect absorber in the visible spectrum, Physical Review B 91 (11) (2015) 115305. arXiv:https://doi.org/10.1103/PhysRevB.91.115305, doi:10.1103/PhysRevB.91.115305.
URL https://doi.org/10.1103/PhysRevB.91.115305

[16] H. Deng, Z. Li, L. Stan, D. Rosenmann, D. Czaplewski, J. Gao, X. Yang, Broadband perfect absorber based on one ultrathin layer of refractory metal, Optics Letters 40 (11) (2015) 2592–2595. arXiv:https://doi.org/10.1364/OL.40.002592, doi:10.1364/OL.40.002592.
URL https://doi.org/10.1364/OL.40.002592

[17] A. Kay, B. Scherrer, Y. Piekner, K. D. Malviya, D. A. Grave, H. Dotan, A. Rothschild, Film flip and transfer process to enhance light harvesting in ultrathin absorber films on specular back-reflectors, Advanced Materials 30 (35) (2018) 1802781. arXiv:https://doi.org/10.1002/adma.201802781, doi:10.1002/adma.201802781.
URL https://doi.org/10.1002/adma.201802781

[18] Z. Li, S. Butun, K. Aydin, Large-area, lithography-free super absorbers and color filters at visible frequencies using ultrathin metallic films, Acs Photonics 2 (2) (2015) 183–188. arXiv:https://doi.org/10.1021/ph500410u, doi:10.1021/ph500410u.
URL https://doi.org/10.1021/ph500410u

[19] Z. Li, E. Palacios, S. Butun, H. Kocer, K. Aydin, Omnidirectional, broadband light absorption using large-area, ultrathin lossy metallic film coatings, Scientific Reports 5 (1) (2015) 1–8. arXiv:https://doi.org/10.1038/srep15137, doi:10.1038/srep15137.
URL https://doi.org/10.1038/srep15137

[20] J. W. Cleary, R. Soref, J. R. Hendrickson, Long-wave infrared tunable thin-film perfect absorber utilizing highly doped silicon-on-sapphire, Optics Express 21 (16) (2013) 19363–19374. arXiv:https://doi.org/10.1364/OE.21.019363, doi:10.1364/OE.21.019363.
URL https://doi.org/10.1364/OE.21.019363

[21] J. W. Cleary, N. Nader, K. D. Leedy, R. Soref, Tunable short-to mid-infrared perfectly absorbing thin films utilizing conductive zinc oxide on metal, Optical Materials Express 5 (9) (2015) 1898–1909. arXiv:https://doi.org/10.1364/OME.5.001898, doi:10.1364/OME.5.001898.
URL https://doi.org/10.1364/OME.5.001898

[22] Q. Wulan, D. He, T. Zhang, H. Peng, L. Liu, V. V. Medvedev, Z. Liu, Salisbury screen absorbers using epsilon-near-zero substrate, Materials Research Express 8 (1) (2021) 016406. arXiv:https://doi.org/10.1088/2053-1591/abd8a1, doi:10.1088/2053-1591/abd8a1.
URL https://doi.org/10.1088/2053-1591/abd8a1

[23] A. Ghobadi, H. Hajian, M. Gokbayrak, B. Butun, E. Ozbay, Bismuth-based metamaterials: from narrowband reflective color filter to extremely broadband near perfect absorber, Nanophotonics 8 (5) (2019) 823–832. arXiv:https://doi.org/10.1515/nanoph-2018-0217, doi:10.1515/nanoph-2018-0217.
URL https://doi.org/10.1515/nanoph-2018-0217

[24] V. Medvedev, V. Gubarev, E. Zoethout, N. Novikova, Interference-enhanced absorption of visible and near-infrared radiation in ultrathin film coatings, IEEE Photonics Technology Letters 33 (22) (2021) 1242–1245. arXiv:https://doi.org/10.1109/LPT.2021.3102149, doi:10.1109/LPT.2021.3102149.
URL https://doi.org/10.1109/LPT.2021.3102149

[25] V. V. Medvedev, An epsilon-near-zero-based dallenbach absorber, Optical Materials 123 (2022) 111899. arXiv:https://doi.org/10.1016/j.optmat.2021.111899, doi:10.1016/j.optmat.2021.111899.
URL https://doi.org/10.1016/j.optmat.2021.111899

[26] M. Agrawal, P. Peumans, Broadband optical absorption enhancement through coherent light trapping in thin-film photovoltaic cells, Optics Express 16 (8) (2008) 5385–5396. arXiv:https://doi.org/10.1364/OE.16.005385, doi:10.1364/OE.16.005385.
URL https://doi.org/10.1364/OE.16.005385

[27] M. Serhatlioglu, S. Ayas, N. Biyikli, A. Dana, M. E. Solmaz, Perfectly absorbing ultra thin interference coatings for hydrogen sensing, Optics Letters 41 (8) (2016) 1724–1727. arXiv:https://doi.org/10.1364/OL.41.001724, doi:10.1364/OL.41.001724.
URL https://doi.org/10.1364/OL.41.001724

[28] A. P. Raman, M. A. Anoma, L. Zhu, E. Rephaeli, S. Fan, Passive radiative cooling below ambient air temperature under direct sunlight, Nature 515 (7528) (2014) 540. arXiv:https://doi.org/10.1038/nature13883, doi:10.1038/nature13883.
URL https://doi.org/10.1038/nature13883

[29] Z. Li, S. Butun, K. Aydin, Large-area, lithography-free super absorbers and color filters at visible frequencies using ultrathin metallic films, Acs Photonics 2 (2) (2015) 183–188. arXiv:https://doi.org/10.1021/ph500410u, doi:10.1021/ph500410u.
URL https://doi.org/10.1021/ph500410u

[30] K. V. Sreekanth, S. Sreejith, S. Han, A. Mishra, X. Chen, H. Sun, C. T. Lim, R. Singh, Biosensing with the singular phase of an ultrathin metal-dielectric nanophotonic cavity, Nature Communi-

cations 9 (2018) 369–1–369–8. arXiv:https://doi.org/10.1038/s41467-018-02860-6, doi:10.1038/s41467-018-02860-6.
URL https://doi.org/10.1038/s41467-018-02860-6

[31] L. J. Krayer, E. M. Tennyson, M. S. Leite, J. N. Munday, Near-ir imaging based on hot carrier generation in nanometer-scale optical coatings, ACS Photonics 5 (2) (2018) 306–311. arXiv:https://doi.org/10.1021/acsphotonics.7b01021, doi:10.1021/acsphotonics.7b01021.
URL https://doi.org/10.1021/acsphotonics.7b01021

[32] G. Brucoli, P. Bouchon, R. Haïdar, M. Besbes, H. Benisty, J.-J. Greffet, High efficiency quasi-monochromatic infrared emitter, Applied Physics Letters 104 (8) (2014) 081101. arXiv:https://doi.org/10.1063/1.4866342, doi:10.1063/1.4866342.
URL https://doi.org/10.1063/1.4866342

[33] A. Naqavi, S. P. Loke, M. D. Kelzenberg, D. M. Callahan, T. Tiwald, E. C. Warmann, P. Espinet-González, N. Vaidya, T. A. Roy, J.-S. Huang, et al., Extremely broadband ultralight thermally-emissive optical coatings, Optics Express 26 (14) (2018) 18545–18562. arXiv:https://doi.org/10.1364/OE.26.018545, doi:10.1364/OE.26.018545.
URL https://doi.org/10.1364/OE.26.018545

[34] R. L. Fante, M. T. McCormack, Reflection properties of the salisbury screen, IEEE transactions on Antennas and Propagation 36 (10) (1988) 1443–1454. arXiv:https://doi.org/10.1109/8.8632, doi:10.1109/8.8632.
URL https://doi.org/10.1109/8.8632

[35] Y. Kotsuka, Electromagnetic Wave Absorbers: Detailed Theories and Applications, John Wiley & Sons, 2019. arXiv:https://doi.org/10.1002/9781119564430, doi:10.1002/9781119564430.
URL https://doi.org/10.1002/9781119564430

[36] J.-Y. Jung, J. Y. Park, S. Han, A. S. Weling, D. P. Neikirk, Wavelength-selective infrared salisbury screen absorber, Applied Optics 53 (11) (2014) 2431–2436. arXiv:https://doi.org/10.1364/AO.53.002431, doi:10.1364/AO.53.002431.
URL https://doi.org/10.1364/AO.53.002431

[37] H. Hara, N. Kishi, H. Iwaoka, Silicon bolometer and micro variable infrared filter for CO_2 measurement, in: 2000 IEEE/LEOS International Conference on Optical MEMS (Cat. No.00EX399), 2000, pp. 139–140. arXiv:https://doi.org/10.1109/OMEMS.2000.879664, doi:10.1109/OMEMS.2000.879664.

[38] Y. Wang, B. J. Potter, J. J. Talghader, Coupled absorption filters for thermal detectors, Optics letters 31 (13) (2006) 1945–1947. arXiv:https://doi.org/10.1364/OL.31.001945, doi:10.1364/OL.31.001945.
URL https://doi.org/10.1364/OL.31.001945

[39] X. Lu, T. Zhang, R. Wan, Y. Xu, C. Zhao, S. Guo, Numerical investigation of narrowband infrared absorber and sensor based on dielectric-metal metasurface, Optics express 26 (8) (2018) 10179–10187. arXiv:https://doi.org/10.1364/OE.26.010179, doi:10.1364/OE.26.010179.
URL https://doi.org/10.1364/OE.26.010179

[40] Y.-L. Liao, Y. Zhao, Ultra-narrowband dielectric metamaterial absorber with ultra-sparse nanowire grids for sensing applications, Scientific reports 10 (2020) 1480–1–1480–7. arXiv:https://doi.org/10.1038/s41598-020-58456-y, doi:10.1038/s41598-020-58456-y.
URL https://doi.org/10.1038/s41598-020-58456-y

[41] M. Nejat, N. Nozhat, Sensing and switching capabilities of a tunable gst-based perfect absorber in near-infrared region, Journal of Physics D: Applied Physics 53 (24) (2020) 245105. arXiv:https://doi.org/10.1088/1361-6463/ab7d6a, doi:10.1088/1361-6463/ab7d6a.
URL https://doi.org/10.1088/1361-6463/ab7d6a

[42] L. Yuan, J. Liao, A. Ren, C. Huang, C. Ji, J. Wu, X. Luo, Ultra-narrow-band infrared absorbers based on surface plasmon resonance, Plasmonics 16 (4) (2021) 1165–1174. arXiv:https://doi.org/10.1007/s11468-021-01384-y, doi:10.1007/s11468-021-01384-y.
URL https://doi.org/10.1007/s11468-021-01384-y

[43] P. Virtanen, R. Gommers, T. E. Oliphant, M. Haberland, T. Reddy, D. Cournapeau, E. Burovski, P. Peterson, W. Weckesser, J. Bright, S. J. van der Walt, M. Brett, J. Wilson, K. J. Millman, N. Mayorov, A. R. J. Nelson, E. Jones, R. Kern, E. Larson, C. J. Carey, İ. Polat, Y. Feng, E. W. Moore, J. VanderPlas, D. Laxalde, J. Perktold, R. Cimrman, I. Henriksen, E. A. Quintero, C. R. Harris, A. M. Archibald, A. H. Ribeiro, F. Pedregosa, P. van Mulbregt, SciPy 1.0 Contributors, SciPy 1.0: Fundamental Algorithms for Scientific Computing in Python, Nature Methods 17 (2020) 261–272. arXiv:https://doi.org/10.1038/s41592-019-0686-2, doi:10.1038/s41592-019-0686-2.

[44] D. T. Pierce, W. E. Spicer, Electronic structure of amorphous si from photoemission and optical studies, Phys. Rev. B 5 (1972) 3017–3029. arXiv:https://doi.org/10.1103/PhysRevB.5.3017, doi:10.1103/PhysRevB.5.3017.
URL https://link.aps.org/doi/10.1103/PhysRevB.5.3017

[45] T. Amotchkina, M. Trubetskov, D. Hahner, V. Pervak, Characterization of e-beam evaporated Ge, YbF_3, ZnS, and LaF_3 thin films for laser-oriented coatings, Applied Optics 59 (5) (2020) A40–A47. arXiv:https://doi.org/10.1364/AO.59.000A40, doi:10.1364/AO.59.000A40.
URL https://doi.org/10.1364/AO.59.000A40

[46] J. I. Larruquert, A. P. Pérez-Marín, S. García-Cortés, L. Rodríguez-de Marcos, J. A. Aznárez, J. A. Méndez, Self-consistent optical constants of SiC thin films, JOSA A 28 (11) (2011) 2340–2345. arXiv:https://doi.org/10.1364/JOSAA.28.002340, doi:10.1364/JOSAA.28.002340.
URL https://doi.org/10.1364/JOSAA.28.002340

[47] J. Kischkat, S. Peters, B. Gruska, M. Semtsiv, M. Chashnikova, M. Klinkmüller, O. Fedosenko, S. Machulik, A. Aleksandrova, G. Monastyrskyi, et al., Mid-infrared optical properties of thin films of aluminum oxide, titanium dioxide, silicon dioxide, aluminum nitride, and silicon nitride, Applied optics 51 (28) (2012) 6789–6798. arXiv:https://doi.org/10.1364/AO.51.006789, doi:10.1364/AO.51.006789.
URL https://doi.org/10.1364/AO.51.006789

[48] P.-K. Chung, S.-T. Yen, Extraction of infrared optical constants from fringing reflectance spectra, Journal of Applied Physics 116 (15) (2014) 153101. arXiv:https://doi.org/10.1063/1.4898037, doi:10.1063/1.4898037.
URL https://doi.org/10.1063/1.4898037

[49] C. C. Katsidis, D. I. Siapkas, General transfer-matrix method for optical multilayer systems with coherent, partially coherent, and incoherent interference, Applied Optics 41 (19) (2002) 3978–3987. arXiv:https://doi.org/10.1364/AO.41.003978, doi:10.1364/AO.41.003978.
URL https://doi.org/10.1364/AO.41.003978

[50] E. D. Palik, Handbook of optical constants of solids, Academic press, 1998.

Viacheslav Medvedev organized this research project. He performed design calculations for light-absorbing coatings and chose the optimal parameters for the deposition of test samples. Viacheslav also wrote the manuscript. Erwin performed test sample deposition, ellipometric and XRR measurements. He also wrote and edited the manuscript. Nadezhda Novikova measured the reflectance spectra of the samples.

Declaration of interests

The authors declare that they have no known competing financial interests or personal relationships that could have appeared to influence the work reported in this paper.